Distinct Behaviors between Gypsum and Silica Scaling in Membrane Distillation Kofi S.S. Christie1†, Yiming Yin2†, Shihong Lin1,3*, and Tiezheng Tong2* Submitted to: *Environmental Science & Technology* 1Department of Civil and Environmental Engineering, Vanderbilt University, Nashville, TN 37212, United States 2Department of Civil and Environmental Engineering, Colorado State University, Fort Collins, CO 80523, United States 3Department of Chemical and Biomolecular Engineering, Vanderbilt University, Nashville, TN 37212, United States † Those authors contributed equally. Corresponding authors: Shihong Lin, shihong.lin@vanderbilt.edu Tiezheng Tong, tiezheng.tong@colostate.edu

ABSTRACT

21

22

23

24

25

26

27

28

29

30

31

32

33

34

35

36

37

38

39

40

Mineral scaling constrains membrane distillation (MD) and limits its application in treating hypersaline wastewater. Addressing this challenge requires enhanced fundamental understanding of the scaling phenomenon. However, MD scaling with different types of scalants may have distinctive mechanisms and consequences which have not been systematically investigated in the literature. In this work, we compared gypsum and silica scaling in MD and demonstrated that gypsum scaling caused earlier water flux decline and induced membrane wetting that was not observed in silica scaling. Microscopic imaging and elemental mapping revealed contrasting scale morphology and distribution for gypsum and silica, respectively. Notably, while gypsum crystals grew both on the membrane surface and deep in the membrane matrix, silica only formed on the membrane surface in the form of a relatively thin film composed of connected sub-micron silica particles. We attribute the intrusion of gypsum into membrane pores to the crystallization pressure as a result of rapid, oriented crystal growth, which leads to pore deformation and the subsequent membrane wetting. In contrast, the silica scale layer was formed via polymerization of silicic acid and gelation of silica particles, which were less intrusive and had a milder effect on membrane pore structure. This hypothesis was supported by the result of tensile testing, which showed that the MD membrane was significantly weakened by gypsum scaling. The fact that different scaling mechanisms could yield different consequences on membrane performance provides valuable insights for the future development of cost-effective strategies for scaling control.

INTRODUCTION

Membrane distillation (MD) is an emerging water separation process suitable for the treatment of hypersaline wastewater.¹⁻⁵ In MD, a vapor pressure gradient generated between a heated feed solution and a cool distillate drives the transport of water vapor across a microporous hydrophobic membrane.⁶ MD possesses several advantages compared to other desalination technologies such as reverse osmosis (RO) and mechanical vapor compression (MVC).⁷ MD tolerates high salinity wastewater that cannot be desalinated by RO and requires lower temperature and capital costs than MVC.¹, ⁷, ⁸ Also, MD is capable of leveraging low-grade waste heat,⁹, ¹⁰ with its modularity rendering it adaptable to the dynamic wastewater treatment demand in industrial applications. These desirable features make MD a promising technological candidate for treating hypersaline wastewater from different industrial sectors.

Despite its desirable features for hypersaline wastewater management, MD has yet to be adopted widely in practice in part due to its vulnerability to membrane-related process failure. Like all other membrane processes, including those that have been extensively employed in practice (e.g., RO and nanofiltration), MD is subject to membrane fouling that results in flux decline. A unique challenge to MD is the wetting of membrane pores when the feed water contains a considerable level of amphiphilic molecules or low-surface-tension, water miscible contaminants. Fortunately, these problems can be satisfactorily addressed either by extensive pretreatment of the feed water 11-14 and/or by using novel membranes with special wettability.1, 15-21 What remains to be an important challenge is membrane scaling, which is particularly problematic if MD is to be used in its most promising application of recovering water from hypersaline wastewater.

As a long-standing challenge facing MD, membrane scaling involves the development of inorganic salt deposits on membrane surfaces.13, 22, 23 During membrane scaling, scalants block membrane pores to cause a reduction in water vapor flux, thereby compromising the process efficiency and economic feasibility of MD. Mineral scaling can lead to pore wetting and the consequent contamination of the distillate.24-26 Compared to organic fouling and pore wetting in MD, a comparable knowledge of inorganic scaling is still emerging,22 and the mechanisms of membrane scaling in the MD process have not been fully understood.27-29 For example, membrane wetting induced by mineral scaling is a mysterious phenomenon. While a previous study has shown that nucleation and subsequent growth of minerals on the membrane surface precede

membrane wetting in vacuum MD experiments with synthetic seawater as the feed solution, the mechanism governing scaling-induced wetting was not clearly elucidated.³⁰ Unlike low-surface-energy or amphiphilic contaminants (e.g., surfactants), which result in membrane wetting by lowering the surface tension of feedwater,³¹, ³² it is still unclear how hydrophobic membranes fail as a barrier to salt transport in MD as a result of mineral scale formation.

Furthermore, due to the complex chemical composition of feedwaters, different types of scaling might occur in an MD process. Gypsum and silica are among the most commonly found scaling in membrane-based desalination. Both types of scaling have been reported in MD as responsible for the dramatic decline of water vapor flux.24, 27, 33, 34 It should be noted that gypsum and silica scaling have distinct formation mechanisms at the molecular level. Gypsum crystals are created via a crystallization process involving the hydrated reaction between Ca2+ and SO42-. In contrast, the formation of silica scale, which is typically amorphous, pertains to the polymerization process of silicic acid.35-37 This fundamental difference might result in varied scaling behaviors in membrane desalination, and a comparative understanding of those behaviors will provide valuable insights to further elucidate the mechanisms of membrane scaling. To the best of our knowledge, however, such a comparison has not been performed in the literature.

In this study, we performed comparative direct-contact membrane distillation (DCMD) experiments with commercial polyvinylidene fluoride (PVDF) membranes using feed solutions that contain the precursors for gypsum and silica formation. The different behaviors of scaling by gypsum and silica were investigated by comparing the water vapor flux, feed salinity, distillate salinity, and transmembrane impedance obtained during DCMD experiments with these two types of scalants. We also characterized the PVDF membranes after the scaling experiments to further elucidate the different mechanisms of scaling. These characterizations included scanning electron microscopy (SEM) to analyze the surface and cross-section morphology of the membranes, energy-dispersive X-ray spectroscopy (EDS) to map the elemental distribution, and tensile testing to understand the impact of scaling on the mechanical strength of the membranes.

MATERIALS AND METHODS

Chemicals and Membranes

Calcium chloride (CaCl₂) and sodium sulfate (Na₂SO₄) were purchased from Research Products International (Mount Prospect, IL). Sodium bicarbonate (NaHCO₃), sodium chloride (NaCl), and

hydrochloric acid (HCl) were acquired from Fisher (Hampton, NH). Sodium metasilicate (Na₂SiO₃) was purchased from Alfa Aesar (Haverhill, MA). All salts and chemicals were used as received without further purification. PVDF membranes with a nominal pore diameter of 0.45 μm were purchased from GE Healthcare (Chicago, IL).

Experimental Setup for Membrane Distillation

We used a custom-built DCMD system to perform MD experiments in this study (Fig. S1, Supporting Information). The feed and distillate streams were circulated by centrifugal pumps through the DCMD cell. The temperatures of the feed and distillate streams were controlled using thermostatic water baths, and were monitored using in-line temperature probes. Throughout the experiments, we measured the mass and electrical conductivity of the distillate, from which we can calculate the real-time flux and salt rejection. We also performed two additional measurements that are not typical in existing DCMD studies. The first measurement was the transmembrane impedance, which was introduced by our previous study to elucidate the surfactant-induced dynamic wetting phenomenon in MD.31,38 Specifically, two 4 cm2 titanium electrodes, one on each side of the membrane, were connected to a potentiostat (Bio-Logic, France). The time-dependent impedance between the two electrodes was measured during the MD experiments. The second additional measurement was feed conductivity, which was monitored by an in-line conductivity probe (eDAQ, Australia). The feed conductivity measurement provides critical information about the saturation level of the feed solution.

Scaling Experiments: Solution Chemistry and Detection Methods

We performed scaling experiments in DCMD using feed solutions of either gypsum or silica. The feed solutions were prepared using solution compositions similar to those used in the literature, which satisfied the criteria of having an initial concentration high enough to offer a reasonable induction time for silica scaling (less than 36 hr for an initial water flux of 25 L m-2 hr-1).36, 39-41 Specifically, gypsum solutions were prepared by mixing CaCl2 and Na2SO4 in deionized water to achieve an initial molar concentration of 24.5 mM for both Ca2+ and SO42- ions, which corresponds to a bulk gypsum saturation index (SI) of 0.16. Silica solutions were prepared by combining 5 mM Na2SiO3, 50 mM NaCl, and 1 mM NaHCO3, then adjusting the pH of the solution to 6.5 using an HCl solution (1 M) to achieve the same SI of 0.16 for amorphous silica. In both cases, the SI was calculated as the logarithm of the quotient of the ion activity products at the supersaturated state (*K*) and the saturation state (*K*₀), respectively:

$$SI = log\left(\frac{K}{K_0}\right)$$
 Eq. 1

PHREEQC, a program developed by the United States Geological Survey to perform aqueous geochemical calculations,⁴² was used to calculate the saturation index of the relevant species within the solutions.

In all scaling experiments, the feed and distillate solution temperatures were maintained at 60 °C and 20 °C, respectively, whereas the flow rates of the feed and distillate streams were controlled as 0.45 L min-1 and 0.3 L min-1, respectively. The feed flow rate was controlled to be higher than the distillate flow rate to enable a slightly higher hydraulic pressure on the feed side of the membrane, which allows for the facile detection of pore wetting. 16, 17 The transmembrane impedance was measured using a sinusoidal perturbation with an amplitude of 5 mV and a frequency of 100 kHz. Each reported impedance data point represents the average of five measurements. Scaling was identified in each experiment by monitoring the water vapor flux over time. The formation of a mineral scale layer blocks the membrane pores, reduces the interfacial area for evaporation, and thus leads to vapor flux decline. We examined the possible occurrence of pore wetting via monitoring the distillate conductivity and the transmembrane impedance over time. As membrane pores become wetted, the penetration of the salty feed solution will result in a measurable increase of the distillate conductivity. Additionally, the progressive migration of the water-air interface (i.e., the thinning of the air-gap in membrane pores) in the dynamic wetting process also results in the change of the transmembrane impedance.

Characterization of Scaled Membranes

To acquire more information regarding how scalants interact with the membranes and how such interactions result in performance failure, we performed detailed characterizations of the membrane samples after the scaling experiments. Both top-view and cross-section micrographs of the scaled membranes were captured using SEM (Zeiss, Germany). Besides, we also performed an elemental analysis of the scaled membranes using EDS. In addition, tensile testing was performed using a mechanical strength testing instrument (Instron, MA) on membrane coupons with a dimension of 5×25 mm to evaluate the impact of scaling on the mechanical strength, which was used to explain the mechanism of pore wetting induced by membrane scaling. Membrane coupons were dried in ambient conditions and gently handled during sample preparation and

tensile testing in which no flaking or peeling of either scalant was observed. At least five replicates of membrane coupons were tested for each sample.

RESULTS AND DISCUSSION

Distinct behaviors between gypsum and silica scaling in MD

The decline of vapor flux over time, as a result of pore blockage by mineral scale on the membrane surface, is a telltale indication of scaling in MD. The scaling induction time is defined as the point at which flux begins to decline. Comparing gypsum and silica feed solutions of equivalent SI (SI=0.16) under identical feed temperature and initial water vapor flux, the induction time for silica scaling was substantially longer than that for gypsum scaling (Fig. 1A vs. 1B, red curves). The flux started to decline immediately after the gypsum scaling experiment started (Fig. 1A), whereas that caused by silica scaling did not occur until ~20 hours (Fig. 1B). We also performed additional experiments with gypsum scaling at a lower SI (SI = 0.05) and observed the stable vapor flux for an extended period of time (Fig. S2), which suggests that gypsum scaling does not have to occur immediately after the experiment starts if the SI is not sufficiently high, and that a reduced initial SI results in a longer induction time. However, we chose to use an SI of 0.16 throughout this study as otherwise the silica scaling experiments would become impractically long.

Further, continuous measurement of the feed conductivity (a surrogate of salinity) revealed that the feed salinity barely changed in the course of gypsum scaling (Fig. 1A). This is because the water flux (and therefore the rate of concentration of the feed solution) was quite low as a result of the short scaling induction time. The feed conductivity decreased slightly at the beginning of the gypsum scaling experiment and then increased very slowly as the MD process continuously removed water from the feed solution via evaporation and thus increased the concentration of NaCl (Fig. S3). On the contrary, the feed conductivity continued to increase throughout the silica scaling experiment (Fig. 1B). In this case, additional 50 mM of NaCl was added with 5 mM Na₂SiO₃ to render the initial feed conductivity comparable to that of gypsum scaling. As a result, the increase of feed salinity was mostly attributable to the long scaling induction time leading to a notable increase of the concentration of the highly soluble NaCl. Starting with a feed conductivity of ~10 mS cm-1, no flux decline was observed until the feed conductivity reached ~20 mS cm-1, which implies that a dramatic increase of resistance against water vapor transport did not occur until total water recovery reached ~50%.

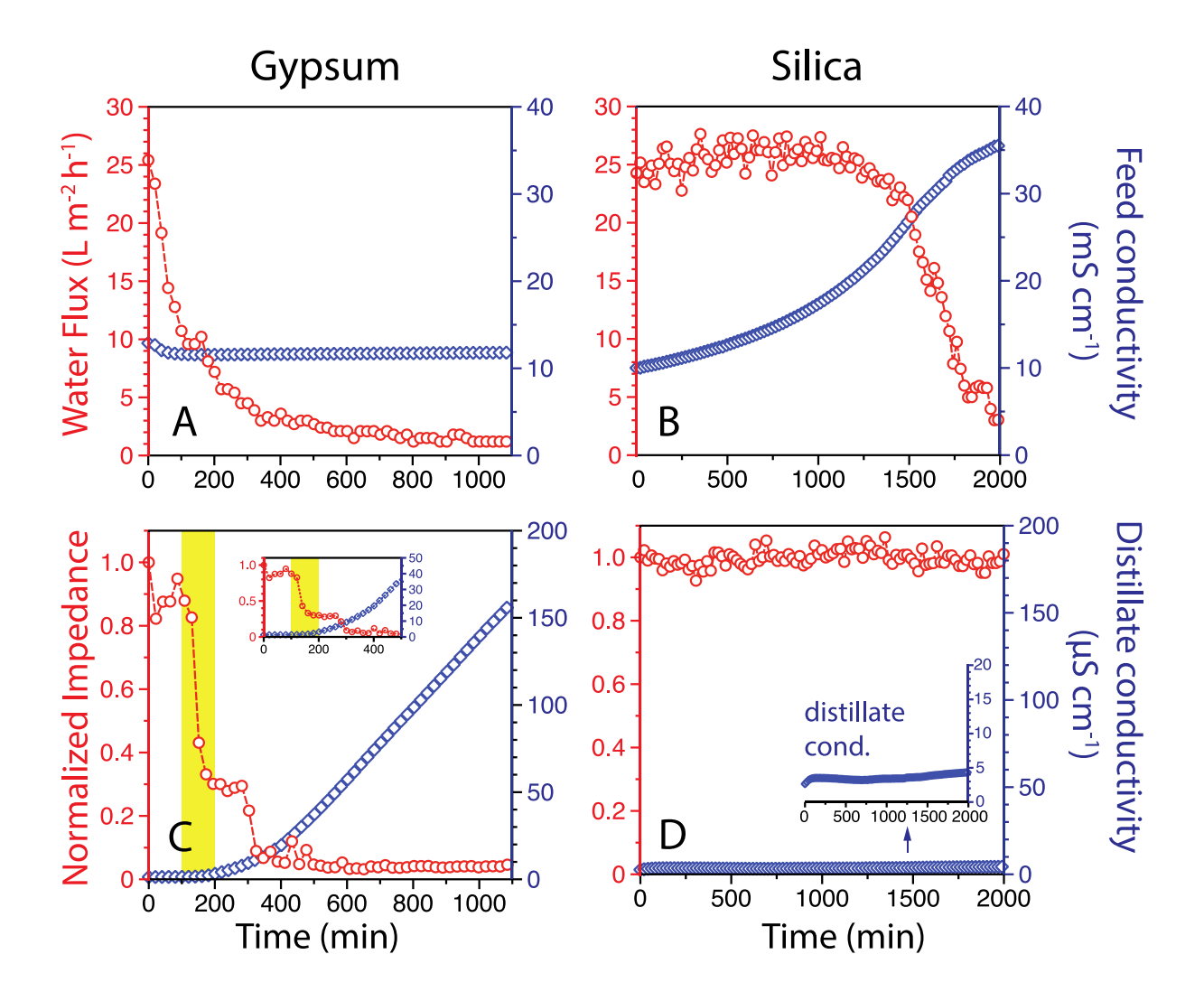


Figure 1. (A and B) Water vapor flux (red) and feed conductivity (blue) in MD experiments with **(A)** gypsum scaling and **(B)** silica scaling. (C and D) Normalized transmembrane impedance at 100 kHz (red) and distillate conductivity (blue) in MD experiments with **(C)** gypsum scaling and **(D)** silica scaling. The initial pH of the feed solution was 6.5 in both cases. The gypsum feed solution had an initial gypsum SI of 0.16. The silica feed solution had an initial silica SI of 0.16. Figure 1A is also replotted as Figure S3 to more clearly show the small change of feed conductivity.

Besides the different scaling kinetics, another notable difference in the behavior of gypsum and silica scaling was whether pore wetting resulted from membrane scaling. Specifically, our experimental results suggest that pore wetting resulted from gypsum scaling but not from silica scaling (Fig. 1). An obvious indication of pore wetting is the increase of distillate conductivity caused by the permeation of salt through the wetted pores. In experiments of gypsum scaling, the distillate conductivity started to increase in about three hours from the beginning of the experiment. The pore wetting induced by gypsum scaling continued to worsen as more water was recovered,

with the real-time rejection decreasing from 98.7% at 200 min to 63.8% at 800 min. Similar differences between gypsum and silica scaling (i.e., earlier water flux decline and unique membrane wetting of gypsum scaling) were also observed in independent experiments using another commercial PVDF membrane (HVHP Durapore, Millipore Sigma) as shown in Fig. S4 (Supporting Information).

The single-frequency (100 kHz) impendence across the membrane was also monitored during the scaling experiments. In our previous studies of pore wetting induced by surfactants, the single-frequency impedance was found to be capable of monitoring imminent wetting before any salts enter the distillate stream.31, 38 Briefly, the progression of the feedwater-air interface within the pores toward the distillate changes the capacitance of the system and thereby results in a shift of impedance. Although the mechanism of wetting induced by surfactants and by mineral scale may be fundamentally different, similar behavior of impedance was observed in our experiments with gypsum scaling. Specifically, the impedance dropped dramatically before significant increase in distillate conductivity was observed (Fig. 1C), which suggests that the feed-air interface within the membrane pores propagated toward the distillate progressively, in the time-scale of tens of minutes (see highlighted range in Fig. 1C) and before any membrane pore was fully penetrated by the feed solution. In contrast to gypsum scaling, silica scaling did not result in any observable pore wetting, even though the DCMD experiment of silica scaling was performed for a much longer time than that of gypsum scaling. Both the distillate conductivity and the single-frequency impedance remained constant throughout the MD experiment (Fig. 3D).

Microscopic characterization of scaled membranes

The PVDF membranes after gypsum scaling and silica scaling demonstrated distinct surface morphologies (Fig. 2). Compared to the pristine PVDF membrane (Fig. S5, Supporting Information), the surface of the PVDF membrane after gypsum scaling was covered by a layer of needle-like gypsum crystals with a magnitude of 100 µm (Fig. 2A). While these distinct crystal particles physically overlapped each other, they did not form a single, chemically connected network. In contrast, the surface of the PVDF membrane after silica scaling showed an amorphous feature, with the sizes of silica particles much smaller than those of gypsum crystals (Fig. 2B). Unlike the growth of gypsum, which follows a crystallization mechanism, the growth of silica follows a gelation mechanism that tends to form a continuous film which consists of submicronsized, chemically bound silica particles (Fig. 2B inset).

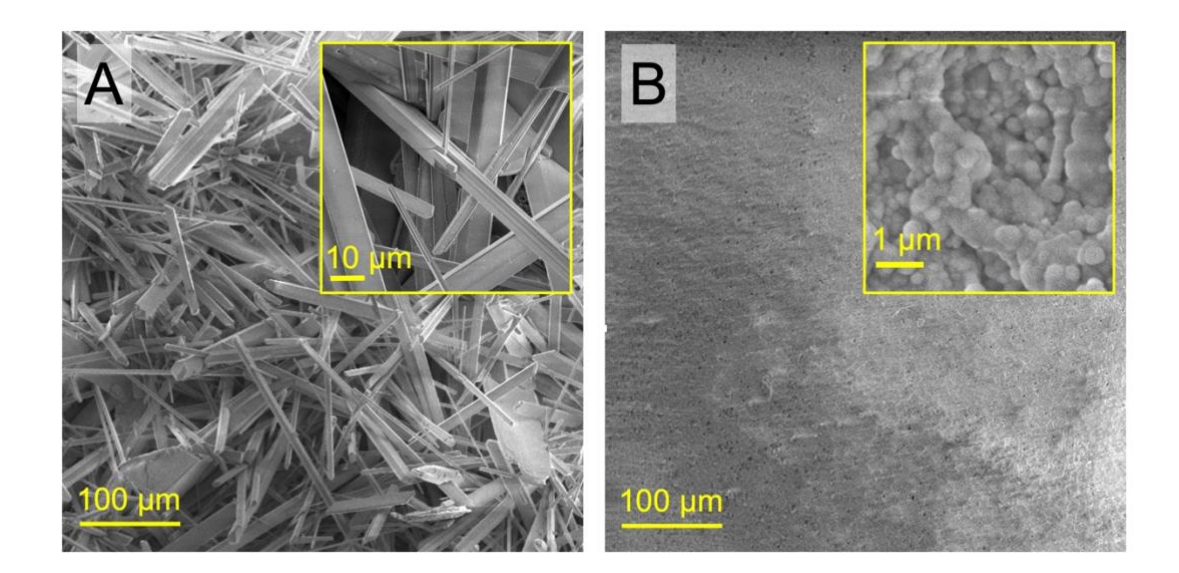


Figure 2. Top-down scanning electron microscope (SEM) images of a polyvinylidene fluoride (PVDF) membrane scaled with **(A)** gypsum and **(B)** silica.

The occurrence of pore wetting induced by gypsum scaling was corroborated by the cross-section micrographs of SEM, which reveals the intrusion of gypsum crystals into the pores of the scaled PVDF membrane (Fig. 3A to 3E). More importantly, flaky gypsum crystals (indicated by the green arrows) were present deep within the PVDF membrane substrate (Fig. 3C). The formation of gypsum both on the surface and within the pores of PVDF membrane was confirmed by the presence of Ca and S elements detected in the EDS analysis (Fig. 3B, 3D, and 3E). On the other hand, no intrusion of silica into the pores of the scaled PVDF membrane was observed. Both the SEM micrograph (Fig. 3F) and the corresponding EDS mapping of Si element (Fig. 3G) suggest that the silica scale was only formed on the top surface of the PVDF membrane without intruding into the membrane pores. Also, the silica scale layer was much thinner than the gypsum scale layer, which was congruent with the slower kinetics of flux reduction due to silica scaling observed in Fig. 1.

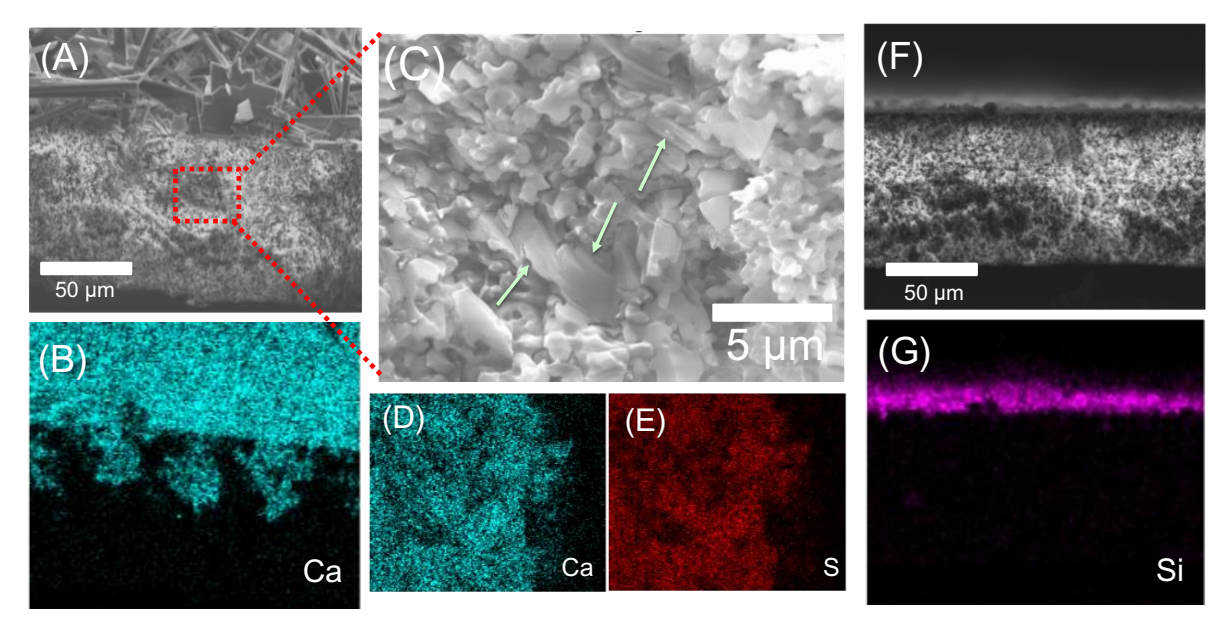


Figure 3. SEM cross-section micrographs (A, C, and F) and the corresponding EDS mapping (B, D, E, and G) for PVDF membrane after gypsum scaling (A to E) and silica scaling (F and G). Panel C is a magnified view of the highlighted region in panel 3A, with its EDS mapping presented in Panels D and E. The green arrows in panel C indicate flaky gypsum crystals observed deep within the membrane substrate.

Mechanisms of the difference between gypsum and silica scaling in MD

The dramatic difference in the behaviors between gypsum and silica scaling was attributable to their distinct scaling mechanisms. The different scaling kinetics (Fig. 1) was likely a result of slower rate of silicic acid polymerization than that of gypsum crystallization, as evidenced by the generally much smaller sizes of silica scale observed in other desalination processes (e.g., RO and forward osmosis)³⁹⁻⁴¹, ⁴³⁻⁴⁵ as well as our microscopic analysis (Fig. 2 and 3). As reported by Mbogoro *et al.*⁴⁶, the growth rate of a single gypsum crystal was ~0.05 μm min-1 for the most reactive [001] facet, using initial Ca₂₊ and SO₄₂₋ concentrations lower than that used in our experiments. Thus, gypsum crystals formed with a high kinetic rate were able to block the membrane pores (nominal diameter of 0.45 μm) quickly and reduce water vapor flux promptly. In contrast, the kinetics of silicic acid polymerization is much slower. Gilron *et al.*³⁴ demonstrated that nanoscale silica particles could be observed after >10 hours of DCMD scaling experiment, with the SI of silica comparable to that of this study. Similarly, silica particles with sizes of 200-500 nm were observed after 2,000 min of silica scaling in the current study, forming a scaling layer that was much thinner than that by gypsum scaling (Fig. 2 and 3). The slow kinetics of silica scaling delayed the onset of water flux decline relative to that with gypsum scaling.

The even more intriguing phenomenon is the distinct wetting behaviors between gypsum and silica scaling in MD. The results of both distillate conductivity and transmembrane impedance indicate that pore wetting was induced by gypsum scaling but not by silica scaling. Although pore wetting induced by low-surface-tension or amphiphilic contaminants (e.g., surfactants) has attracted considerable attention and has been investigated extensively in the literature, 31, 32, 47 whether membrane wetting would occur concomitantly with mineral scaling remains uncertain. Also, the mechanism of scaling-induced wetting (when it indeed occurs) is ambiguous. It has been demonstrated that surfactants promote membrane wetting by reducing the surface tension of the feed solutions. 31, 32 In such cases, pore wetting occurs when the liquid entry pressure (LEP) becomes lower than the hydraulic pressure difference, ΔP . In the case of scaling, however, the heightened feed salinity (as more water is recovered) increases the surface tension of feed solution and the corresponding LEP if all other factors are assumed to be unchanged. 48 Therefore, other mechanism(s) must exist for wetting that is induced by mineral scaling.

At the wetting frontier within the membrane pores, there are several possible interfaces for the addition of new crystal mass by precipitating out solutes from the feed solution. These interfaces include the water-membrane interface, the water-air interface, and the water-crystal interface. Thermodynamics of crystallization suggest that an interface with a lower interfacial energy also has a lower Gibbs free energy of crystallization and is thus more favorable for crystal growth.49,50 Thus, crystal growth at the water-air interface, which possesses the highest interfacial energy, is as unfavorable as homogeneous precipitation,51 while the growth of a crystal that has already formed is the most favorable. Consequently, gypsum crystals near the wetting frontier can grow bigger in the confined space within the membrane pores (Fig. 4A). A similar but more-widely studied phenomenon is crystal growth in porous media, such as stone and concrete. Previous studies in this field have found that crystal growth in microscopic confined space can impose a substantial "crystallization pressure" against the confining "walls",52-55 causing cracking and damage to buildings and geotechnical structures. The crystallization pressure, ΔP , can be quantified ass6

$$\Delta P = \frac{vRT}{V_m} SI$$
 Eq. 2

where v is the van't Hoff factor of the solute (v = 2 for gypsum), R is the ideal gas constant, T is the absolute temperature, and V_m is the molar volume of the solid crystal (\sim 73.8 cm³ mol-1 for

gypsum). For gypsum, vRT/V_m is as high as ~75.0 J cm-3 at 60 °C, which suggests that gypsum can theoretically exert an enormous pressure (~12 MPa at SI=0.16) against the membrane pores even at a relatively low level of supersaturation.

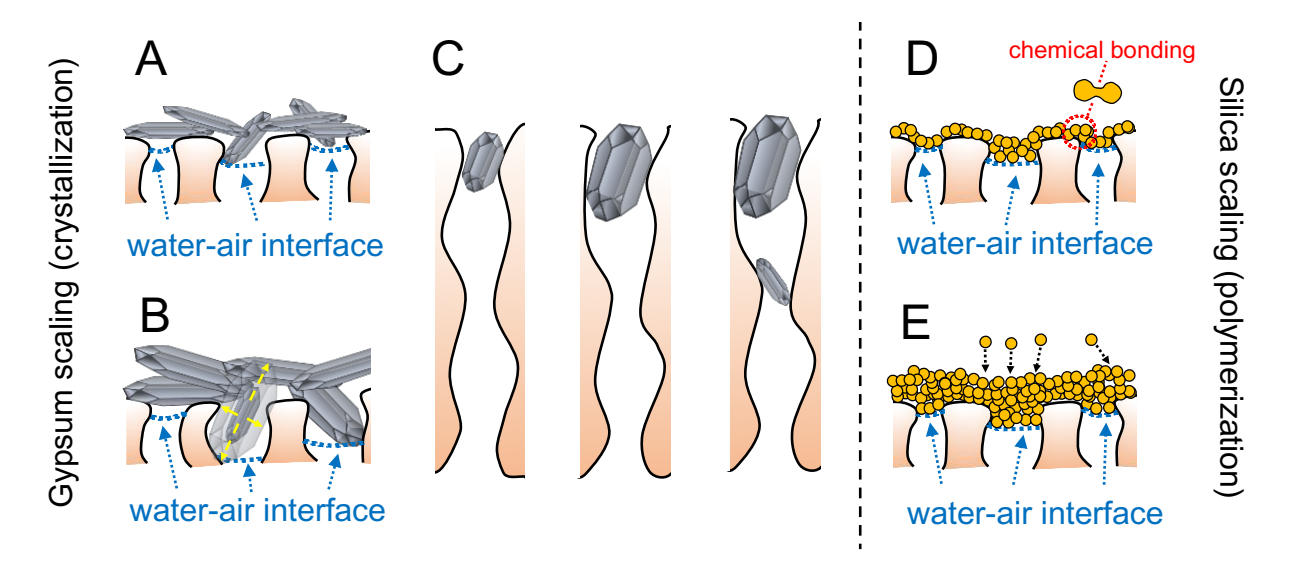


Figure 4. Schematic illustration of **(A)** Initial formation of gypsum crystal particles near the wetting frontier before any wetting occurs; **(B)** Pore deformation caused by local growth of gypsum crystals that exert a large crystallization pressure; **(C)** Mechanism of wetting frontier propagation: the deformation of pores near the entrance results in reduced LEP and movement of the wetting frontier. The crystal growth at the new wetting frontier will again lead to local pore deformation and further movement of the wetting frontier; **(D)** Formation of a silica "mat" that covers the membrane pores; **(E)** Thickening of the silica "mat" by deposition of more silica particles and the further polymerization of silicic acid onto the formed silica "mat."

The water-crystal interface possesses the lowest interfacial energy due to the hydrophilic nature of gypsum crystals. Therefore, the water-crystal interface is most preferable for precipitating out additional solutes from the solution. Among all crystal particles that have already formed in the system, those near the wetting frontier are particularly prone to further growth because the local *SI* is the highest due to concentration polarization driven by evaporative flux (Fig. 4A). Therefore, it is expected that the fastest crystal growth occurs to the crystals located near the wetting frontier, which locally deforms the membrane pores (Fig. 4B). The local deformation of membrane pores results in an increase of membrane pore size and reduction of LEP (Fig. 4C). If the local LEP is lower than the hydraulic pressure, wetting occurs and the water-air interface propagates toward the distillate until it reaches a small aperture with a corresponding local LEP that again exceeds the hydraulic pressure.

The exact mechanism for the new water-air interface to continue its propagation toward the distillate needs further elucidation. It is possible that smaller crystals begin to grow in the region near the new wetting frontier (Fig. 3C and 4C), and the crystallization pressure eventually leads to sufficient expansion of the aperture at the current wetting frontier so that the wetting frontier can move to the next position with a smaller aperture. This process of local deformation by crystallization pressure repeats itself, which eventually leads to percolation of the feedwater across the membrane (i.e., wetting). This theoretical postulation of the mechanism for crystallization-induced pore wetting suggests that such a wetting process is progressive, which is consistent with results observed in Fig. 1C. Specifically, the time difference between the onset of impedance drop and the onset of distillate conductivity increase was in the order of tens of minutes for wetting induced by gypsum scaling.

However, this mechanism of pore deformation due to crystallization pressure as described above does not apply to silica scaling which does not involve crystal growth. The formation of the silica scale layer follows two major steps. The first step is the polymerization of silicic acid to form silica particles,57 and the second step is gelation in which silica particles aggregate to form a cake layer on the membrane surface (Fig. 2B and 4D).58,59 Together, these two steps lead to the formation of a silica "mat" in which the primary particles are chemically bonded with each other. Different from gypsum crystals, silica particles are amorphous and lack of orientation preference for growth. The scaling precursors (i.e., silicate) in the feed solution grows the scale layer either by forming more silica particles that later deposit onto the existing scale layer, or by further polymerizing on the existing scale layer to make it thicker (Fig. 4E). However, due to the lack of orientation preference for polymerization growth, the silica scale layer stays as a film on the membrane surface rather than forcefully intruding into the membrane pores (Fig. 3F and 3G). Therefore, the scaling by silica did not induce pore wetting in MD.

If this hypothesis of pore deformation by gypsum crystallization is correct, we should expect the mechanical properties of the PVDF membrane to be significantly affected by gypsum scaling. Therefore, we performed tensile testing of three PVDF membrane samples, including the reference membrane after an MD experiment using deionized (DI) water (without any scalant), the membrane after an MD experiment with silica scaling, and the membrane after an MD experiment with gypsum scaling. The experimental conditions of the MD experiments with scaling were

identical to those for Fig. 1. The representative stress-strain curves for these different samples are presented in Fig. 5A.

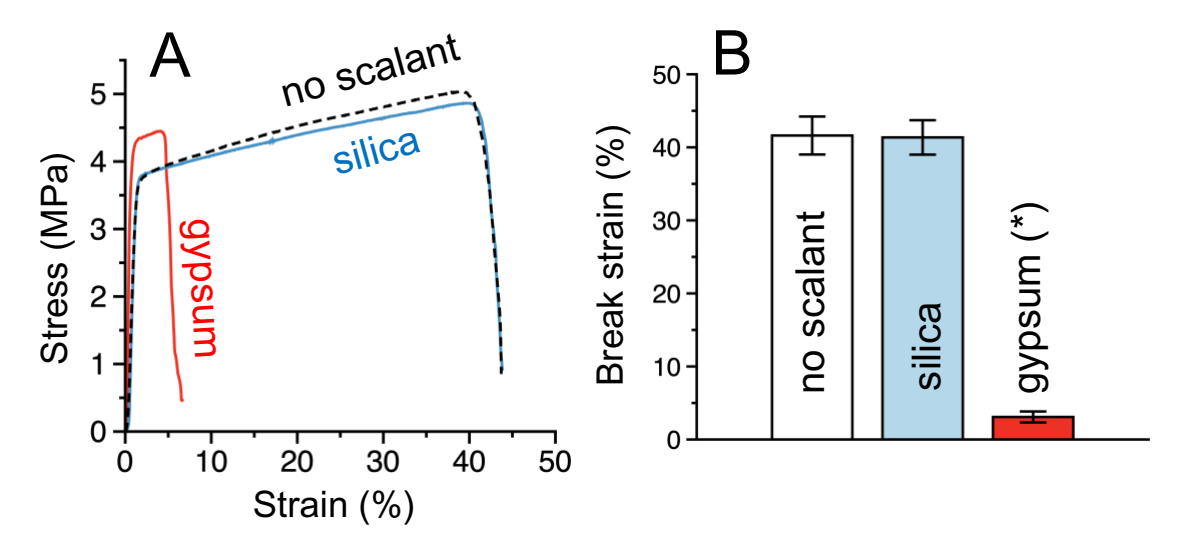


Figure 5. (A) Stress-strain curves for three different membrane samples, including the PVDF membrane after an MD experiment with deionized water (dash black), as well as the PVDF membranes subject to silica scaling (blue) and gypsum scaling (red). **(B)** Summary of the break point strain for the three membrane samples. Error bars represent standard deviations from five measurements. The asterisk (*) indicate that the break strain of a gypsum-scaled membrane was statistically different from a membrane subjected to an MD experiment without scalant (p < 10-5).

Comparing the representative stress-strain curves for the three membrane samples suggest that gypsum scaling significantly reduces the break point strain (i.e., the percent of membrane elongation upon fracture) as compared to the reference membrane subject to an MD experiment with DI water. In contrast, silica scaling does not seem to have any observable impact on the tensile properties of the PVDF membrane (Fig. 5A). Statistical analysis (with five replicates for each sample) also confirms the break point strains for the reference membrane and membrane subject to silica scaling are similar and are both significantly higher than the membrane subject to gypsum scaling (Fig. 5B). The decrease in break strain was likely associated with the increased pore sizes within membrane substrate due to pore deformation. Similarly, a decrease of break point strain caused by the increased depth and width of the voids within the polymer matrix has been observed in other studies.60-62 Interestingly, scaling of either kind does not seem to reduce the break point stress (i.e., the stress upon fracture, Fig. 5A and Table S1), which suggests that the most salient effect of gypsum scaling was to make the membrane more brittle. Overall, gypsum scaling reduced

the toughness the membrane, which is proportional to the area under the stress-strain curve, i.e., the integral of stress with respect to strain (Table S1).

IMPLICATIONS

We have demonstrated contrasting behaviors between gypsum scaling and silica scaling in MD desalination. Gypsum scaling caused much earlier decline of water flux and induced membrane wetting that was not observed in silica scaling. Although it is known that these two scalants are produced from different mechanisms, i.e., crystallization and polymerization for gypsum scaling and silica scaling, respectively, our comparative experiments reveal, for the first time, that this mechanistic difference can translate to dramatically different impacts on membrane performance. In inland brackish water desalination where the saturation index of gypsum is typically higher than, or comparable to, that of silica,63,64 gypsum scaling is more prone to initiate the water vapor flux decline while the detrimental effect of silica scaling on water productivity is not expected to occur until the feed solution is concentrated to a much greater extent. Even worse, gypsum scaling also has an additional detrimental effect of scaling-induced pore wetting. These considerations imply that cost-effective measures for scaling control, whether via pretreatment to remove scaling precursors, adding anti-scalant chemicals, or developing scaling-resistant membranes, should probably be prioritized toward mitigating scalants which are formed through crystallization.

ACKNOWLEDGEMENTS

The authors acknowledge that this material is based upon work supported by the National Science Foundation Graduate Research Fellowship Program (award number DGE-1445197). T.T. acknowledges the support from the start-up funds received from the Department of Civil and Environmental Engineering, College of Engineering at Colorado State University, and the Bureau of Reclamation (USBR) under the Department of Interior via DWPR Agreement R18AC00108. S.L. acknowledges the support from National Science Foundation via research grant CBET-1705048.

ASSOCIATED CONTENT

Supporting Information

Schematic of the MD setup for impedance measurements (Figure S1); Experimental results (water flux and distillate conductivity) for gypsum scaling with an initial SI of 0.05 (Figure S2); Experimental results

- in Figure 1A replotted using a narrower range of feed conductivity (Figure S3); Experimental results for
- 405 gypsum and silica scaling with an initial SI of 0.16 but with a PVDF membrane of a different brand
- 406 (Millipore Sigma) from that used in the main text (Figure S4); Scanning electron microscopy image of the
- 407 pristine PVDF membrane (Figure S5); Summary of mechanical properties from tensile testing (Table S1)

408

409

AUTHOR CONTRIBUTIONS

410 K.C. and Y.Y. contributed equally to this work.

411 DISCLOSURE

The authors declare no competing financial interest.

413 REFERENCES

- 1. Deshmukh, A.; Boo, C.; Karanikola, V.; Lin, S. H.; Straub, A. P.; Tong, T. Z.;
- Warsinger, D. M.; Elimelech, M., Membrane distillation at the water-energy nexus: limits,
- opportunities, and challenges. *Energy & Environmental Science* **2018**, *11*, 1177-1196.
- 2. Dongare, P. D.; Alabastri, A.; Pedersen, S.; Zodrow, K. R.; Hogan, N. J.; Neumann, O.;
- Wu, J. J.; Wang, T. X.; Deshmukh, A.; Elimelech, M.; Li, Q. L.; Nordlander, P.; Halas, N. J.,
- Nanophotonics-enabled solar membrane distillation for off-grid water purification. *P Natl Acad*
- 420 *Sci USA* **2017**, *114* (27), 6936-6941.
- Thomas, N.; Mavukkandy, M. O.; Loutatidou, S.; Arafat, H. A., Membrane distillation
- research & implementation: Lessons from the past five decades. Sep Purif Technol 2017, 189, 108-
- 423 127.
- 424 4. Alkhudhiri, A.; Darwish, N.; Hilal, N., Membrane distillation: A comprehensive review.
- 425 Desalination **2012**, 287, 2-18.
- 426 5. Wang, W.; Du, X. W.; Vahabi, H.; Zhao, S.; Yin, Y. M.; Kota, A. K.; Tong, T. Z.,
- Trade-off in membrane distillation with monolithic omniphobic membranes. *Nat Commun* **2019**,
- 428 *10*.
- 429 6. Lawson, K. W.; Lloyd, D. R., Membrane distillation. *J Membrane Sci* **1997**, *124* (1), 1-25.
- 430 7. Tong, T. Z.; Elimelech, M., The Global Rise of Zero Liquid Discharge for Wastewater
- 431 Management: Drivers, Technologies, and Future Directions. *Environ Sci Technol* **2016**, *50* (13),
- 432 6846-6855.
- 433 8. Chang, H.; Li, T.; Liu, B.; Vidic, R.; Elimelech, M.; Crittenden, J. C., Potential and
- implemented membrane-based technologies for the treatment and reuse of flowback and produced
- water from shale gas and oil plays: A review. *Desalination* **2019**, *455*, 34-57.
- 436 9. Shaffer, D. L.; Chavez, L. H. A.; Ben-Sasson, M.; Castrillon, S. R. V.; Yip, N. Y.;
- 437 Elimelech, M., Desalination and Reuse of High-Salinity Shale Gas Produced Water: Drivers,
- 438 Technologies, and Future Directions. *Environ. Sci. Technol.* **2013**, 47 (17), 9569-9583.
- 439 10. Lokare, O. R.; Tavakkoli, S.; Wadekar, S.; Khanna, V.; Vidic, R. D., Fouling in direct
- contact membrane distillation of produced water from unconventional gas extraction. *J Membrane*
- 441 *Sci* **2017,** *524*, 493-501.

- 442 11. Gryta, M., Fouling in direct contact membrane distillation process. *J Membrane Sci* **2008**,
- 443 *325* (1), 383-394.
- 444 12. Wang, J.; Qu, D.; Tie, M.; Ren, H. J.; Peng, X. J.; Luan, Z. K., Effect of coagulation
- pretreatment on membrane distillation process for desalination of recirculating cooling water. *Sep*
- 446 *Purif Technol* **2008**, *64* (1), 108-115.
- 13. Tijing, L. D.; Woo, Y. C.; Choi, J. S.; Lee, S.; Kim, S. H.; Shon, H. K., Fouling and its
- control in membrane distillation-A review. *J Membrane Sci* **2015**, *475*, 215-244.
- 2449 14. Zhang, Z. Y.; Du, X. W.; Carlson, K. H.; Robbins, C. A.; Tong, T. Z., Effective treatment
- of shale oil and gas produced water by membrane distillation coupled with precipitative softening
- and walnut shell filtration. *Desalination* **2019**, *454*, 82-90.
- 452 15. Wang, Z. X.; Elimelech, M.; Lin, S. H., Environmental Applications of Interfacial
- 453 Materials with Special Wettability. *Environ Sci Technol* **2016**, *50* (5), 2132-2150.
- Lin, S. H.; Nejati, S.; Boo, C.; Hu, Y. X.; Osuji, C. O.; Ehmelech, M., Omniphobic
- 455 Membrane for Robust Membrane Distillation. *Environmental Science & Technology Letters* **2014**,
- 456 *1* (11), 443-447.
- 457 17. Lee, J.; Boo, C.; Ryu, W. H.; Taylor, A. D.; Elimelech, M., Development of Omniphobic
- 458 Desalination Membranes Using a Charged Electrospun Nanofiber Scaffold. *Acs Appl Mater Inter*
- **2016,** *8* (17), 11154-11161.
- 460 18. Wang, Z. X.; Hou, D. Y.; Lin, S. H., Composite Membrane with Underwater-Oleophobic
- Surface for Anti-Oil-Fouling Membrane Distillation. Environ Sci Technol 2016, 50 (7), 3866-
- 462 3874.
- 463 19. Wang, Z. X.; Lin, S. H., Membrane fouling and wetting in membrane distillation and their
- mitigation by novel membranes with special wettability. *Water Res* **2017**, *112*, 38-47.
- 465 20. Huang, Y. X.; Wang, Z. X.; Jin, J.; Lin, S. H., Novel Janus Membrane for Membrane
- 466 Distillation with Simultaneous Fouling and Wetting Resistance. Environ Sci Technol 2017, 51
- 467 (22), 13304-13310.
- 468 21. Li, C. X.; Li, X. S.; Du, X. W.; Tong, T. Z.; Cath, T. Y.; Lee, J., Antiwetting and
- 469 Antifouling Janus Membrane for Desalination of Saline Oily Wastewater by Membrane
- 470 Distillation. Acs Appl Mater Inter **2019**, 11 (20), 18456-18465.
- 471 22. Tong, T. Z.; Wallace, A. F.; Zhao, S.; Wang, Z., Mineral scaling in membrane
- desalination: Mechanisms, mitigation strategies, and feasibility of scaling-resistant membranes. J
- 473 *Membrane Sci* **2019**, *579*, 52-69.
- 474 23. Warsinger, D. M.; Swarninathan, J.; Guillen-Burrieza, E.; Arafat, H. A.; Lienhard, J. H.,
- Scaling and fouling in membrane distillation for desalination applications: A review. *Desalination*
- **2015**, *356*, 294-313.
- 477 24. Karanikola, V.; Boo, C.; Rolf, J.; Elimelech, M., Engineered Slippery Surface to Mitigate
- 478 Gypsum Scaling in Membrane Distillation for Treatment of Hypersaline Industrial Wastewaters.
- 479 Environ Sci Technol **2018**, *52* (24), 14362-14370.
- 480 25. Rezaei, M.; Warsinger, D. M.; Lienhard, J. H.; Duke, M. C.; Matsuura, T.; Samhaber,
- W. M., Wetting phenomena in membrane distillation: Mechanisms, reversal, and prevention.
- 482 *Water Res* **2018,** *139*, 329-352.
- 483 26. Gryta, M., Calcium sulphate scaling in membrane distillation process. *Chem Pap* **2009**, *63*
- 484 (2), 146-151.
- 485 27. Xiao, Z. C.; Li, Z. S.; Guo, H.; Liu, Y. J.; Wang, Y. S.; Yin, H. B.; Li, X. M.; Song, J.
- 486 F.; Nghiem, L. D.; He, T., Scaling mitigation in membrane distillation: From superhydrophobic
- 487 to slippery. *Desalination* **2019**, *466*, 36-43.

- 488 28. Xiao, Z. C.; Zheng, R.; Liu, Y. J.; He, H. L.; Yuan, X. F.; Ji, Y. H.; Li, D. D.; Yin, H.
- 489 B.; Zhang, Y. B.; Li, X. M.; He, T., Slippery for scaling resistance in membrane distillation: A
- 490 novel porous micropillared superhydrophobic surface. *Water Res* **2019**, *155*, 152-161.
- 491 29. Su, C. L.; Horseman, T.; Cao, H. B.; Christie, K.; Li, Y. P.; Lin, S. H., Robust
- 492 Superhydrophobic Membrane for Membrane Distillation with Excellent Scaling Resistance.
- 493 Environ Sci Technol **2019**, *53*,11801-11809.
- 494 30. Kiefer, F.; Präbst, A.; Rodewald, K. S.; Sattelmayer, T., Membrane scaling in Vacuum
- Membrane Distillation Part 1: In-situ observation of crystal growth and membrane wetting. J
- 496 *Membrane Sci* **2019**, *590*.117305
- 497 31. Wang, Z. X.; Chen, Y. M. L.; Sun, X. M.; Duddu, R.; Lin, S. H., Mechanism of pore
- wetting in membrane distillation with alcohol vs. surfactant. *J Membrane Sci* **2018**, *559*, 183-195.
- 499 32. Wang, Z. X.; Chen, Y. M. L.; Lin, S. H., Kinetic model for surfactant-induced pore wetting
- in membrane distillation. *J Membrane Sci* **2018,** *564*, 275-288.
- Bush, J. A.; Vanneste, J.; Gustafson, E. M.; Waechter, C. A.; Jassby, D.; Turchi, C. S.;
- Cath, T. Y., Prevention and management of silica scaling in membrane distillation using pH
- 503 adjustment. *J Membrane Sci* **2018**, *554*, 366-377.
- 504 34. Gilron, J.; Ladizansky, Y.; Korin, E., Silica Fouling in Direct Contact Membrane
- 505 Distillation. *Ind Eng Chem Res* **2013**, *52* (31), 10521-10529.
- Neofofistou, E.; Demadis, K. D., Use of antiscalants for mitigation of silica (SiO2) fouling
- and deposition: fundamentals and applications in desalination systems. Desalination 2004, 167 (1-
- 508 3), 257-272.
- 509 36. Tong, T. Z.; Zhao, S.; Boo, C.; Hashmi, S. M.; Elimelech, M., Relating Silica Scaling in
- Reverse Osmosis to Membrane Surface Properties. *Environ Sci Technol* **2017,** *51* (8), 4396-4406.
- 511 37. Yin, Y. M.; Wang, W.; Kota, A. K.; Zhao, S.; Tong, T. Z., Elucidating mechanisms of
- silica scaling in membrane distillation: Effects of membrane surface wettability. *Environ Sci*:
- 513 *Water Res Technol* **2019**, *5*, 2004-2014.
- 514 38. Chen, Y. M. L.; Wang, Z. X.; Jennings, G. K.; Lin, S. H., Probing Pore Wetting in
- Membrane Distillation Using Impedance: Early Detection and Mechanism of Surfactant-Induced
- 516 Wetting. *Environ Sci Tech Let* **2017**, *4* (11), 505-510.
- 517 39. Mi, B. X.; Elimelech, M., Gypsum Scaling and Cleaning in Forward Osmosis:
- 518 Measurements and Mechanisms. *Environ Sci Technol* **2010**, 44 (6), 2022-2028.
- 519 40. Mi, B. X.; Elimelech, M., Silica scaling and scaling reversibility in forward osmosis.
- 520 *Desalination* **2013,** *312*, 75-81.
- 521 41. Xie, M.; Gray, S. R., Gypsum scaling in forward osmosis: Role of membrane surface
- 522 chemistry. *J Membrane Sci* **2016,** *513*, 250-259.
- 523 42. Parkhurst, D.; Appelo, C. A. J. User's Guide to PHREEQC (version 2) A computer
- 524 program for speciation, batch-reaction, one-dimensional transport, and inverse geochemical
- *calculations*; U.S. Geological Survey Water-Resources Investigations Report 99-4259: 1999.
- 526 43. Uchymiak, M.; Lyster, E.; Glater, J.; Cohen, Y., Kinetics of gypsum crystal growth on a
- 527 reverse osmosis membrane. *J Membrane Sci* **2008,** *314* (1-2), 163-172.
- 528 44. Thompson, J.; Rahardianto, A.; Kim, S.; Bilal, M.; Breckenridge, R.; Cohen, Y., Real-
- 529 time direct detection of silica scaling on RO membranes. *J Membrane Sci* **2017,** *528*, 346-358.
- 530 45. Xie, M.; Gray, S. R., Silica scaling in forward osmosis: From solution to membrane
- interface. Water Res **2017**, 108, 232-239.
- 532 46. Mbogoro, M. M.; Peruffo, M.; Adobes-Vidal, M.; Field, E. L.; O'Connell, M. A.; Unwin,
- P. R., Quantitative 3D Visualization of the Growth of Individual Gypsum Microcrystals: Effect of

- Ca2+:SO42- Ratio on Kinetics and Crystal Morphology. J Phys Chem C 2017, 121 (23), 12726-
- 535 12734.
- Wang, Z. X.; Chen, Y. M. L.; Zhang, F. Y.; Lin, S. H., Significance of surface excess
- 537 concentration in the kinetics of surfactant-induced pore wetting in membrane distillation.
- 538 Desalination **2019**, 450, 46-53.
- 539 48. Wang, X. X.; Chen, C. C.; Binder, K.; Kuhn, U.; Poschl, U.; Su, H.; Cheng, Y. F.,
- Molecular dynamics simulation of the surface tension of aqueous sodium chloride: from dilute to
- 541 highly supersaturated solutions and molten salt. *Atmos Chem Phys* **2018**, *18* (23), 17077-17086.
- 542 49. Christenson, H. K., Two-step crystal nucleation via capillary condensation. *Crystengcomm*
- **2013,** *15* (11), 2030-2039.
- 544 50. Kashchiev, D.; Firoozabadi, A., Nucleation of gas hydrates. J Cryst Growth 2002, 243 (3-
- 545 4), 476-489.
- 546 51. Wu, W. J.; Nancollas, G. H., Interfacial free energies and crystallization in aqueous media.
- 547 J Colloid Interf Sci 1996, 182 (2), 365-373.
- 548 52. Correns, C. W., Growth and Dissolution of Crystals under Linear Pressure. Discuss
- 549 *Faraday Soc* **1949**, (5), 267-271.
- 550 53. Xie, P.; Beaudoin, J. J., Mechanism of Sulfate Expansion .1. Thermodynamic Principle of
- 551 Crystallization Pressure. Cement Concrete Res 1992, 22 (4), 631-640.
- 552 54. Scherer, G. W., Stress from crystallization of salt. Cement Concrete Res 2004, 34 (9), 1613-
- 553 1624.
- 55. Flatt, R. J.; Steiger, M.; Scherer, G. W., A commented translation of the paper by C.W.
- Correns and W. Steinborn on crystallization pressure. *Environ Geol* **2007,** *52* (2), 221-237.
- 556 56. Steiger, M., Crystal growth in porous materials I: The crystallization pressure of large
- 557 crystals. J Cryst Growth **2005**, 282 (3-4), 455-469.
- 558 57. Belton, D. J.; Deschaume, O.; Perry, C. C., An overview of the fundamentals of the
- chemistry of silica with relevance to biosilicification and technological advances. Febs J 2012,
- 560 *279* (10), 1710-1720.
- 58. Brinker, C. J.; Scherer, G. W., Sol-]Gel-]Glass .1. Gelation and Gel Structure. J Non-Cryst
- 562 *Solids* **1985,** 70 (3), 301-322.
- 563 59. Dietler, G.; Aubert, C.; Cannell, D. S.; Wiltzius, P., Gelation of Colloidal Silica. *Phys Rev*
- 564 *Lett* **1986,** *57* (24), 3117-3120.
- 565 60. Lai, C. Y.; Groth, A.; Gray, S.; Duke, M., Preparation and characterization of
- poly(vinylidene fluoride)/nanoclay nanocomposite flat sheet membranes for abrasion resistance.
- 567 *Water Res* **2014,** *57*, 56-66.
- 568 61. Tsai, H. A.; Hong, M. J.; Huang, G. S.; Wang, Y. C.; Li, C. L.; Lee, K. R.; Lai, J. Y.,
- 569 Effect of DGDE additive on the morphology and pervaporation performances of asymmetric PSf
- 570 hollow fiber membranes. *J Membrane Sci* **2002**, *208* (1-2), 233-245.
- 571 62. Shi, L.; Wang, R.; Cao, Y. M.; Feng, C. S.; Liang, D. T.; Tay, J. H., Fabrication of
- 572 poly(vinylidene fluoride-co-hexafluropropylene) (PVDF-HFP) asymmetric microporous hollow
- 573 fiber membranes. *J Membrane Sci* **2007**, *305* (1-2), 215-225.
- 574 63. Bond, R.; Veerapaneni, S. Zero Liquid Discharge for Inland Desalination; Awwa Research
- 575 Foundation: 2007.
- 576 64. Inc., T. T. Analysis of Water From Four Wells at the Brackish Groundwater National
- 577 Desalination Research Facility; U.S. Department of the Interior, Bureau of Reclamation, Brackish
- 578 Groundwater National Desalination Research Facility: New Mexico, 2011.

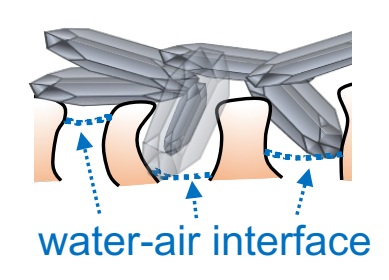
TOC Art

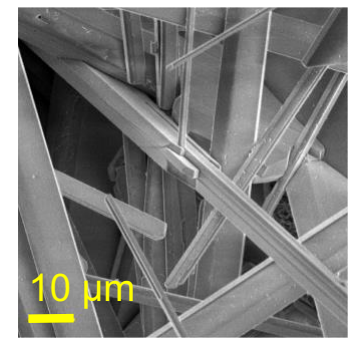
580

Gypsum vs. Silica Scaling in Membrane Distillation

Oriented crystal growth

Gypsum



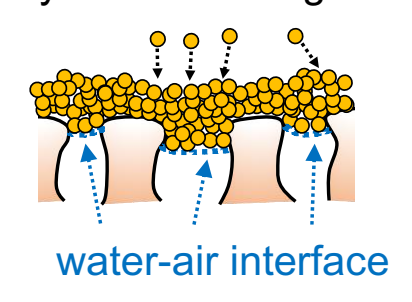


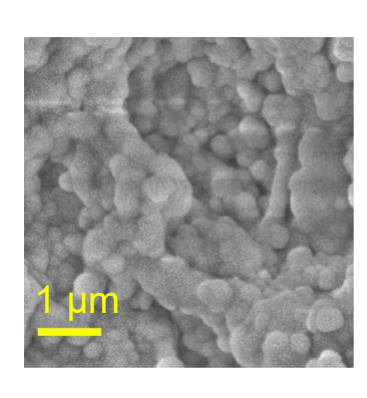
- Faster
- Intrusive
- Induce wetting

Polymerization & gelation

Silica

581 582





- Slower
- Stay on surface
- Does not induce wetting